Neutron studies of the structure and dynamics of molecular and polymer self-assembled systems

Vasily T Lebedev[1]**, Yuri V Kulvelis**[1]**, Sergey S Ivanchev**[2]**, Alexander Ya Vul**[3]**, Alexander I Kuklin**[4]**, Oleg N Primachenko**[2] **and Alexey S Odinokov**[2]

[1] B.P.Konstantinov Petersburg Nuclear Physics Institute, NRC Kurchatov Institute, Gatchina, Leningrad distr., Russia
[2] Institute of Macromolecular Compounds of RAS, Saint-Petersburg, Russia
[3] Ioffe Institute, Saint-Petersburg, Russia
[4] Joint Institute for Nuclear Research, Dubna, Russia

E-mail: lebedev_vt@pnpi.nrcki.ru

Abstract

Structures of perfluorinated polymer membranes in dry and wet state and their molecular dynamics have been studied by neutron small angle scattering and neutron spin echo. In swolen membranes there were observed proton conducting channels ($\sim$1–2 nm in diameter) being branched fractals (dimension $\sim$2.2–2.6). In these structures, in the experimental time-interval $t = 0$–150 ps, the detected fast dynamics reflected mainly water diffusion mixed with protons' hopping from one water molecule to another during proton exchange between ionic groups SO_3H in side chains of macromolecules. To reinforce the channels' system and proton conductivity, the membranes' modification was developed by embedding nanodiamonds with hydrophilic surface since in aqueous solutions they create gel networks with the cells of $\sim$40 nm in size. In composite membranes a dopation with nanodiamons (size $\sim$4–5 nm, concentration $\leqslant$1%wt) has stimulated proton conductivity at the enhanced temperatures (20 °C–50 °C).

Keywords: membrane, proton, conductivity, diamond, neutron, structure, dynamics

(Some figures may appear in colour only in the online journal)

1. Introduction

Design of proton conducting membranes is aimed at obtaining better and stable conductivity in combination with higher mechanical characteristics and maintaining necessary water contents at higher temperatures needed to prevent catalysts' poisoning in fuel elements [1, 2]. Modern ion conducting materials are based mainly on perfluorinated polymers (figure 1) forming membrane films in sedimentation processes from the solutions (Nafion®) or by using aqueous emulsions (Aquivion®) [3, 4]. Usually the Nafion® type membranes with polymer having long side chains (figure 1) work at the temperatures lower 90 °C and lose functional properties above. The development of new technologies to produce the Aquivion® type copolymers with short side chains (figure 1) promises to increase the temperatures of fuel elements exploitation (higher 130 °C) in order to use a cheaper hydrogen of lower purity without any risks of catalysts poisoning that prolongs the working period of hydrogen cells.

On the other hand, the functional properties of these materials can be improved by their modification with various nanoparticles (e.g. SiO_2, TiO_2) introduced into polymer matrix to enhance proton conductivity and strength, mechanical and electrical stability by heating during exploitation [5, 6]. The membranes' modification by doping with the nanodiamonds is especially promising way due to their unique physical and chemical characteristics (highest thermal conductivity, chemical resistance, hardness etc) [7, 8]. Along with this, detonation nanodiamonds (DND, size $\sim$4–5 nm) have very developed
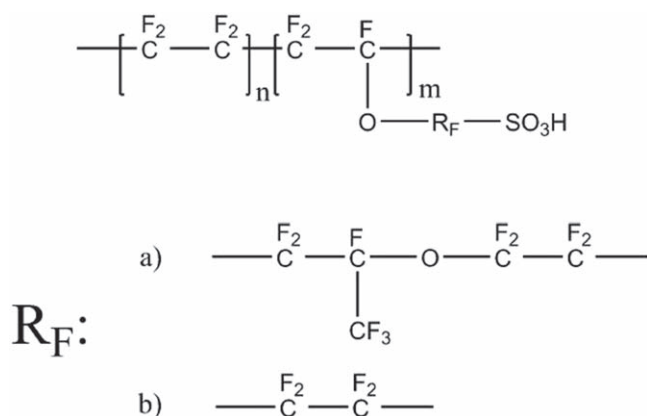
Figure 1. Chemical structure of perfluorinated polymers: (a) long side chains (Nafion); (b) short side chains (Aquivion).

surface which can be cleaned from graphite fragments and then grafted with the functional groups (COOH, OH, H) to get necessary charge (positive or negative ζ-potential) of the particles in aqueous media that enables to regulate their assembly (formation of chains, branched aggregates and gel-like structures) [9, 10]. Such DND crystals may be assembled also by the interaction with polymers in solutions, and there are various opportunities to design the composite membranes where labile formations of diamond particles are fixed in polymer matrix by solvent removal. The effective way to obtain highly ordered membranes with advanced functional properties should be based on a fundamental knowledge of the criteria defining optimal conditions of materials' synthesis. Along with the studies of structural regularities defining the formation of composites it is relevant a research of proton dynamics in wet membranes as dependent on their structure. In these materials a system of channels provides water percolation. Therefore it is possible a transfer of protons linked with water molecules by hydrogen bonds and also hopping protons from a molecule to molecule (Grotthus mechanism) [11]. Our work is devoted to the comprehensive analysis of membrane materials and their components in neutron structural and dynamical experiments and the application of the results to design new composite membranes improved by diamonds inserted.

2. Experimental

2.1. Samples and methods

Perfluorinated polymers have been synthesized by the aqueous emulsion method [2]. There were studied the membrane films (dry and saturated with light or heavy water, thickness of a single film $\sim$0.05 mm) by Small angle neutron scattering (SANS) ('YuMO' spectrometer, JINR, Dubna) [12, 13]. The intensities of scattering from the samples were normalized to the data of the measurements with vanadium standard for calibration using the program SAS package [14]. The experiments at ambient temperature (20 °C) in the range of momentum transfer $q = 0.04$–5 nm^{-1} have covered the spatial scales $R \sim 2\pi/q \sim 1$–100 nm at which the main features of

polymer chains ordering are revealed. This allowed observe the channels for water percolation in dry and swollen materials and to examine the subtle structural features of polymer packing in partially crystalline matrices with a segregation of hydrophobic and hydrophilic (backbone and side chain) fragments. In SANS-studies we used the polymers with different equivalent weights (EW = 800 and 1000 g mol^{-1}) those are the weights of chain fragments between neighbouring SO$_3$H groups. On the samples we carried out also the experiments on molecular dynamics by resonant Neutron Spin-Echo (spectrometer MUSES, LLB, Saclay) by measuring quasielastic scattering (coherent, incoherent) on water and protons belonging to water molecules and polymer ionic groups. The time and momentum transfer diapasons, $t = 0.6$–150 ps, $q = 10$–18 nm^{-1}, allowed us look for dynamics at the scale comparable to water molecular size by detecting its diffusion and possible proton hopping [11] in membrane channels. At the next stage of the work, we aimed to improve conducting channels in membranes by using hydrophilic nanoparticles to be introduced into polymer matrices. For this purpose, we prepared appropriate aqueous dispersion of nanodiamonds (positively charged, 4–5 nm in size, concentration 1%wt) by five-fold dilution of diamond hydrogel (5%wt) existing above the critical concentration ($c^* \sim 4$%wt). Partially, it was expected a conservation of gel structure in the dispersion at least at nanoscale or submicron scales. This assumption was verified in SANS experiments when the dispersion demonstrated relatively strong diamonds' assembly. It has served as a basement to use the nanodiamonds to prepare the composites with perfuorinated polymer (EW = 800). The membrane films containing nanodiamonds (0.25 and 1.0%wt) we produced by a sedimentation of components from the mixture of polymer and DND in dimethyl-formamide and removing solvent by the method [2]. Then we tested these membrane films in conductivity measurements similar to the procedure described [2].
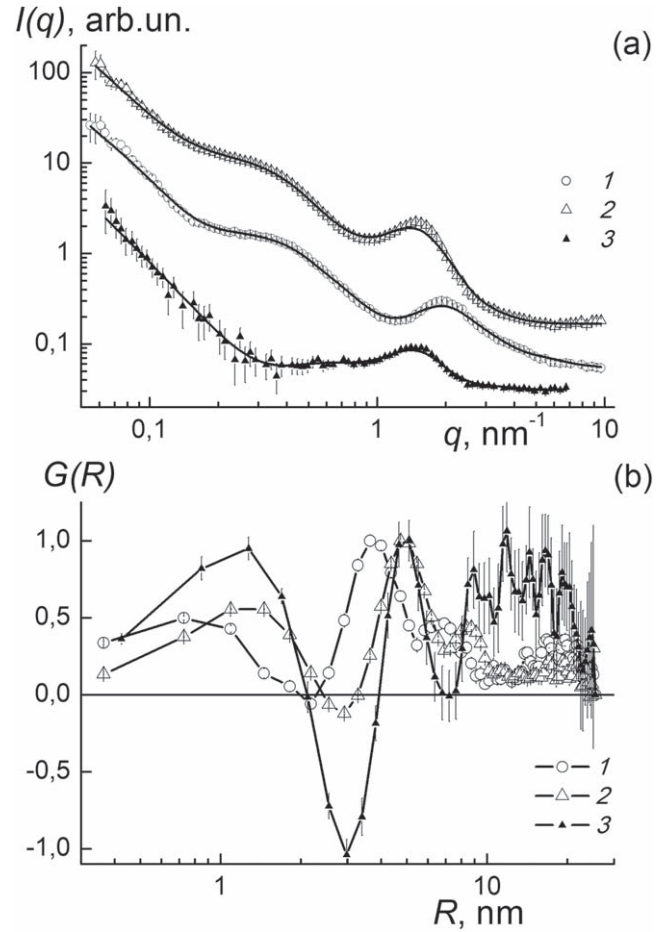
3. Results and discussion

3.1. Structure of polymer membranes by SANS

Membranes (EW = 800;1000) demonstrated neutron scattering stronger by filling with light water (uptake 39%–40% and 16–18%wt) due to its good contrast in relation to the bulk polymer mostly hydrophobic (figures 2(a), 3(a)). This gain against initially dry material indicates also possible expansion of membrane cavities due to water penetration into them. On the other hand, the scattering became lower when the membranes have absorbed heavy water depressing the neutron contrast between cavities and polymer. Thus, the contrast variation has enabled us to visualize nanoscale cavities in polymer matrix. The SANS profiles are qualitatively similar and display the ionomer peak with the position of maximum $q_m \sim 1.3$–2.2 nm^{-1}, a hump at $q_m \sim 0.3$–0.5 nm^{-1} and scattering upturn at lower edge of the q-range (figures 2(a), 3(a)). The ionomer peak indicates a segregation of ionic groups forming the channels covered inside by sulfonic groups which absorb water in wet membranes.
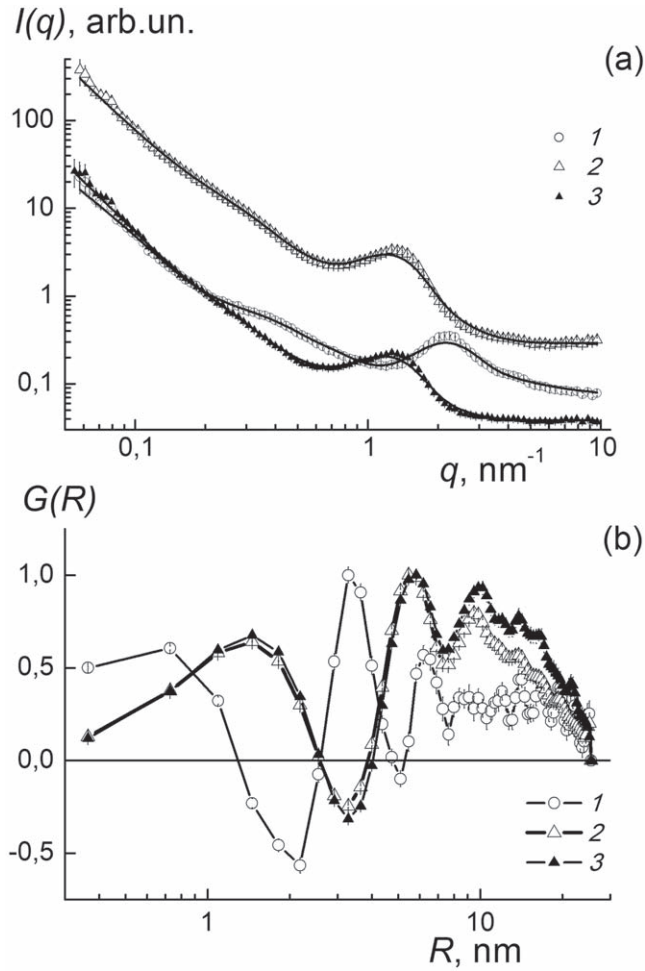
Figure 2. SANS from the membrane (EW = 800) dry (1) and filled with light or heavy water (2, 3): (a)—intensities *I(q)* versus momentum transfer, curves are fitting functions (1); (b)—spectra of correlations *G(R)* versus radii *R*.

Figure 3. SANS from the membrane (EW = 1000) dry (1) and filled with light or heavy water (2,3): (a)—intensities *I(q)* versus momentum transfer, curves are fitting functions (1); (b)—spectra of correlations *G(R)* versus radii *R*.

The local ordering of ionic groups is clear visible by the spectra $G(R) = R^2\gamma(R)$ restored from the data by Fourier-transform (ATSAS software) [15], where the function $\gamma(R)$ describes the pair correlations between centers of scattering (groups, monomer units, water molecules) at the distance R. Here the functions $G(R)$ are normalized to the amplitude of the second maximum in the position $R \sim 3$–5 nm (figures 2(b), 3(b)). In dry membranes the functions $G(R)$ display the first peak with the position of maximum $R_{1D} \sim 0.7$ nm. Membranes' swelling causes a shift of the peak, $R_{1S} \sim 1.3$–1.5 nm. These small radii may serve as a measure of channels' width showing their expanding due to wetting. Simultaneously, it increases the spacing between the channels (second peak), $R_{2D} \sim 3$ nm and $R_{2S} \sim 5$ nm (figures 2(b), 3(b)). Primarily this is evident from a displacement of diffraction maximum at $q_m \sim 1.3$–2.2 nm^{-1} (figures 2(a), 3(a)). These correlated structural changes are explained by swelling hydrophilic regions in membranes. On the other hand, in them there are the domains (size $\sim 2\pi/q_m \sim 15$–20 nm) mostly hydrophobic which are relatively stable since they absorb water weakly. These regions are better visible if the scattering from the channels is damped by filling with heavy water. In this case the

spectra $G(R)$ exhibit intense correlations in the band of $R \sim 10$–20 nm (figures 2(b), 3(b), data 3).

To get more detailed information on the parameters of conducting channels and their arrangement in matrix we built the model scattering function assuming that the channels are thin filaments with transversal gyration radius r_g [16]. The channels are considered as polymer-like coils having fractal geometry with exponent $\beta \sim 2$ [17]. The resulting squared form factor of a channel is the function $F^2(q) \sim (1/q^\beta) \cdot \exp[-(qr_g)^2/2]$ [17, 18]. The factor $(1/q^\beta)$ is the asymptotic form of the scattering function of a mass fractal $I_o/[1 + (q\xi)^2]^{\beta/2}$ where I_o is the forward scattering intensity, and ξ is the correlation length showing the size of fractal object [18]. At high momentum transfer $q \gg 1/\xi$ one can obtain the scattering law A/q^β with a constant $A = I_o/\xi^\beta$ where the scattering intensity $I_o \sim (\Delta K)^2 V_{FR}^{\ 2} N_{FR}$ is proportional to the squared contrast factor of channels in matrix (ΔK), the squared volume of a channel (V_{FR}) and their number in the sample (N_{FR}) [16, 18]. On the other hand, we have taken into account the arrangement of channels in matrix at characteristic distances (L) revealed as maxima (R_{2D}, R_{2S} etc) of correlation functions (figures 2(b), 3(b)). This defines the structure factor $S(q)$ for the ensemble of channels according to Debye formula [16]. Finally, we used the model function to

describe the q-dependence of scattering intensities

$$I(q) = \frac{A}{q^{\beta}} e^{-(qr_g)^2/2} \left(1 + \sum_{i=1}^{k} C_i \frac{\sin qL_i}{qL_i}\right) + B. \qquad (1)$$

This function depends on fitting parameters A, β, r_g, C_i, L_i ($i = 1, 2\ldots6$) characterizing the structure of membranes and the constant B being a contribution of incoherent scattering mainly due to the presence of hydrogen in the samples. The parameter A is defined by the contrast factor (ΔK) of channels which can be empty or filled with water (light, heavy) that modifies strongly the scattering intensity (figures 2(a), 3(a)) and allows to visualize the conducting channels. They have small transversal gyration radii $r_g \sim 0.3$–0.7 nm comparable to the size of a molecule of water. A network of channels is composed of coiled linear fragments with fractal dimension $1 < \beta < 2$ in dry membranes, while in wet state an additional free volume is filled with water and some channels are branched, $2 < \beta < 3$. They are separated by hydrophobic polymer regions of excluded volume ($C_i < 0$) and spaced ($C_i > 0$) at the distances, $L_i \sim 3$–40 nm ($i = 1$, $2\ldots6$). Here the coefficients C_i indicate the presence of different correlations between channels. In the case of zero coefficients there will be observed an independent scattering from the channels. The peculiarities of channels structure and polymer package can depend on the equivalent weight of polymer since the amount of ionic groups regulates the arrangement of hydrophilic and hydrophobic regions in membranes. Fitting with the function (1) (figures 2(a), 3(a)) has given the gyration radii of the channels in dry (r_{gd}) and wet (r_{gH}, r_{gD}) membranes:

> equivalent weight EW = 800,
> $r_{gd} = 0.20 \pm 0.03$ nm, $r_{gH} = 0.49 \pm 0.01$ nm,
> $r_{gD} = 0.60 \pm 0.03$ nm;
>
> EW = 1000,
> $r_{gd} = 0.24 \pm 0.03$ nm, $r_{gH} = 0.52 \pm 0.01$ nm,
> $r_{gD} = 0.38 \pm 0.14$ nm.

The increase of equivalent weight does not change significantly the radii of channels. However, in dry and filled with light water samples (high contrast of channels in matrix) there is weak effect of channels' shrinking due to larger amount of ionic groups at lower EW = 800. All the magnitudes of r_g are smaller the radii $R_{1D} \sim 0.7$–0.8 nm, $R_{1S} \sim 1.3$–1.5 nm at maxima positions (figures 2(b), 3(b)) since the radii reflect local correlations along the channels also. It confirms a local anisotropy of channels being chain-like structures having in dry membranes a low fractal dimension, $\beta_d < 2$:

$$\beta_d = 1.9 \pm 0.1; \ \beta_d = 1.7 \pm 0.1 \text{ for EW} = 800 \text{ and } 1000.$$

These parameters show that at smaller equivalent weight the channels trend to be more coiled due to enhanced electrostatic interactions (larger amount of ionic groups).

By swelling some squeezed cavities in membranes absorb water. It changes the geometry of channels and they become branched with higher fractal index, $\beta_{H,D} > 2$:

$$\beta_H = 2.6 \pm 0.1; \ \beta_D = 2.5 \pm 0.1 \text{ for EW} = 800;$$
$$\beta_H = 2.2 \pm 0.1; \ \beta_D = 2.4 \pm 0.1 \text{ for EW} = 1000.$$

Again, in wet membranes with lower equivalent weight the channels are more branched due to stronger interaction of ionic groups.

In dry membranes locally one can consider the channels as the cylinders having the diameter $d_d = 2\sqrt{2}r_{gd} \sim 0.6$–0.7 nm close the doubled size of water molecules. Hence, water may penetrate into the channels and promote proton migration especially due to the expansion of channels' diameter $d_{H,D} = 2\sqrt{2}r_{gH,D} \sim 1.1$–1.7 nm.

As we found, in membranes the channels are surrounded by hydrophobic shells with the external radius $L_1 \sim 1.6$–1.8 nm in dry state and the enlarged radius $L_1 \sim 2.6$–2.9 nm in wet state. These excluded volume areas define spacing between channels, $L_2 \sim 2L_1 \sim 3.5$–3.6 nm and $L_2 \sim 4.4$–5.2 nm in dry and wet membranes.

A short range order in the arrangement of channels is detected at larger distances also. The excluded volume effects are revealed at the radii $L_3 \sim 3.9$–5.1 nm and 6.1–6.3 nm in dry and wet membranes, and the channels are spaced at bigger distances $L_4 \sim 2L_3 \sim 10$–11 nm and 12–17 nm respectively. Thus, the channels are gathered into the bunches where a given channel is surrounded by another ones lying within the first (L_2) and the second (L_4) coordination spheres. Their diameters increase by swelling. Meanwhile, the hydrophobic domains are spaced at the distances $L_5 \sim 19$–21 nm, $L_6 \sim 30$–34 nm which are weakly changed by wetting.

These structural features are inherent in both polymers (EW = 800; 1000) where a variation of ionic groups' fraction does not cause the qualitative changes in molecular order. Meanwhile, a greater water uptake (39–40%wt) in matrix with lower equivalent weight (EW = 800) stimulates swelling and expansion of channels' bunches comparatively to the samples with lower fraction of ionic groups (EW = 1000) absorbing less water (16–18%wt). Eventually, these subtle distinctions influence on fast molecular dynamics in swollen membranes.

3.2. Molecular dynamics in membranes

In the NSE-experiments (Neutron Resonance Spin Echo, MUSES, LLB, Saclay) we studied molecular dynamics at ambient temperature (20 °C) in the membranes saturated with light water (uptake 72 and 36%wt, EW = 800; 1000). We used the NSE method [19] to detect a quasielastic scattering of polarized neutrons from water molecules and protons to get the information on their mobility in the picosecond time-interval at spatial scales of few molecular diameters. The fundamentals, experimental techniques and theories concerning NSE experiments are developed for the applications in molecular physics and polymer science [20]. In our case, there were determined time-dependent autocorrelations when moving molecule (proton) causes a change in neutron velocity by quasielastic scattering [21]. As a result, it is measured a neutron polarization in the form of NSE-signal $P_{nse}(t) = \exp[-q^2 D_P t]$ showing a decay with a diffusion constant D_P [19–21]. This signal is a polarization of scattered neutrons normalized to initial value (P_o). In general, the $P_{nse}(t)$
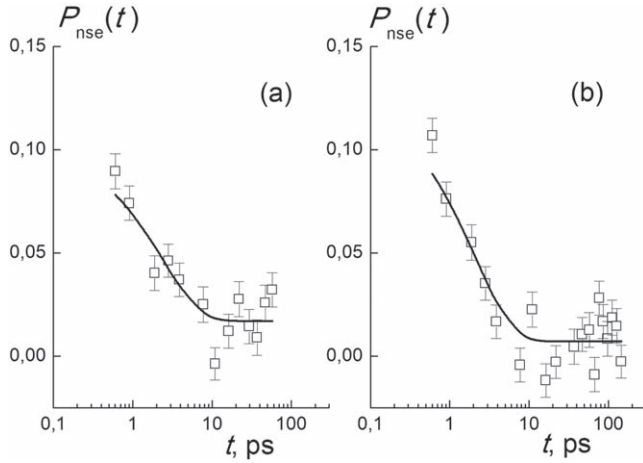
Figure 4. NSE-signals from wet membrane (EW = 800) at $q = 10$ and 14 nm^{-1} (a), (b). Lines are fitting functions (3).

Figure 5. NSE-signals from wet membrane (EW = 1000) at $q = 16$ and 18 nm^{-1} (a), (b). Lines are fitting functions (3).

includes the contributions of inelastic components (σ_{coh}, σ_{inc}) of coherent and incoherent scattering with partial signals $P_{coh}(t)$ and $P_{inc}(t)$ and the part (σ_{el}) related to elastic scattering with a constant signal $P_{el}(t) = 1$. At last a not polarized background (Bg) does not influence on the time-dependence of $P_{nse}(t)$ but reduce the amplitude of measured signal [19]

$$P_{nse}(t) = \frac{\sigma_{coh} \cdot P_{coh}(t) + \sigma_{inc} \cdot P_{inc}(t) + \sigma_{el}}{\sigma_{coh} + \sigma_{inc} + \sigma_{el} + Bg}. \qquad (2)$$

A coherent inelastic scattering on molecules does not cause neutron spin flipping, $P_{coh}(t) > 0$, $P_{coh}(t = 0) = 1$, but the spin incoherence by neutron scattering on protons changes the sign and the amplitude of neutron polarization, $P_{inc}(t) < 0$, $P_{inc}(t = 0) = -1/3$ [19]. These peculiarities define the behaviors of measured NSE-signals.

In our experiments on wet membranes the NSE-data in the time-interval $t = 0.6$–150 ps reflect local motions of water molecules and protons at short scales $r \sim 2\pi/q \sim 0.3$–0.6 nm corresponding to momentum transfer $q = 10$–18 nm^{-1} (figures 4, 5). Since light water has a good contrast against polymer, the coherent scattering from water molecules dominates ($P_{coh}(t) > 0$) that provides the positive NSE-signals, and negative contributions of incoherent scattering on protons ($P_{inc}(t) < 0$) are compensated.

For both membranes the functions $P_{nse}(t)$ show a fast decay at $t \leqslant 10$ ps (figures 4, 5). A plateau at longer times $t \geqslant 10$ ps indicates a slow relaxation processes not resolved in this t-interval (practically elastic part of scattering cross section) (figures 4, 5). The experimental data demonstrate a single relaxation process that is mostly a translational diffusion of water when the protons move together with water molecules and proton hopping seems to be less probable at short times. Therefore, all the data were approximated by a simple function usually used to describe molecular diffusion [19]

$$P_{nse}(q, t) = P_1 \exp(-t/\tau) + P_2, \qquad (3)$$

where the first term represents the correlation function with the amplitude P_1 and relaxation time τ, and the second one is the constant additive P_2 (e.g. long-time relaxation).
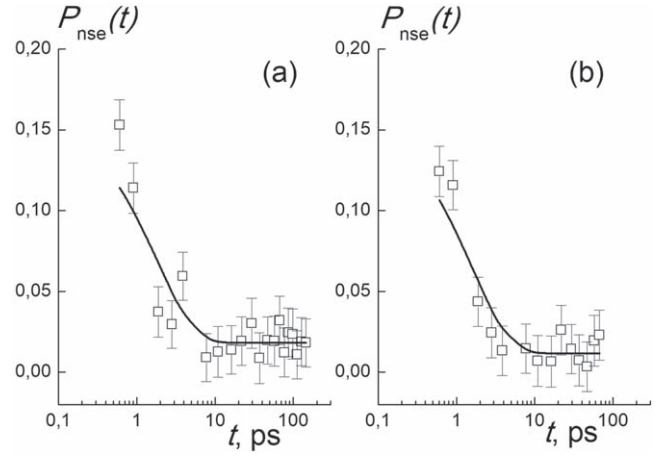
The data approximation with the function (2) has given the inelastic amplitudes $P_1 = [\sigma_{coh} – (1/3)\sigma_{inc})]/[\sigma_{coh} + \sigma_{in} + Bg] \sim 0.1$ much higher the elastic ones, $P_2 = \sigma_{el}/[\sigma_{coh} + \sigma_{in} + Bg] \sim 0.01$.

The dynamic correlations are characterized by the times:

$$\tau_{10} = 2.50 \pm 0.49 \text{ ps}, \tau_{14} = 2.21 \pm 0.38 \text{ ps at}$$
$$q = 10 \text{ and } 14 \text{ nm}^{-1}$$

in the first membrane, EW = 800;

$$\tau_{16} = 1.96 \pm 0.42 \text{ ps}, \tau_{18} = 1.72 \pm 0.35 \text{ ps at}$$
$$q = 16 \text{ and } 18 \text{ nm}^{-1}.$$

in the second membrane, EW = 1000.

For a set of the parameters we found the effective diffusion constants $D_{eff} = 1/(\tau q^2)$ which are comparable to the constant $D_W = 2.3 \times 10^{-5}$ cm^2 s^{-1} for bulk water diffusion at ambient temperature [21]:

$$D_{10} = (4.00 \pm 0.80) \cdot 10^{-5} \text{ cm}^2 \text{ s}^{-1},$$
$$D_{14} = (2.31 \pm 0.40) \cdot 10^{-5} \text{ cm}^2 \text{ s}^{-1},$$
$$q = 10; 14 \text{ nm}^{-1};$$
$$D_{16} = (1.99 \pm 0.43) \cdot 10^{-5} \text{ cm}^2 \text{ s}^{-1},$$
$$D_{18} = (2.27 \pm 0.46) \cdot 10^{-5} \text{ cm}^2 \text{ s}^{-1},$$
$$q = 16; 18 \text{ nm}^{-1}.$$

For both membranes the data D_{eff} are presented in figure 6. In these membranes with similar structural organization we neglected subtle differences in the diffusion and analyzed the data together. Totally the data show the increase of diffusion rate at larger scales $r = 2\pi/q$ from single to doubled size of water molecule. At lower scale, $r \sim 0.3$ nm $\sim$ water molecule diameter, it is visible a mobility in narrow channels predominantly, where water is partially immobilized on the walls (solvation on sulfonic groups). However, at larger scale $r \sim 0.6$ nm a volume mobility of water is more revealed and proton hopping may contribute to observed dynamics also [11].

This is important for proton conductivity since in polymer chains each SO$_3$H-group is separated from the neighboring groups by 4 or 7 chain units. A direct protons exchange
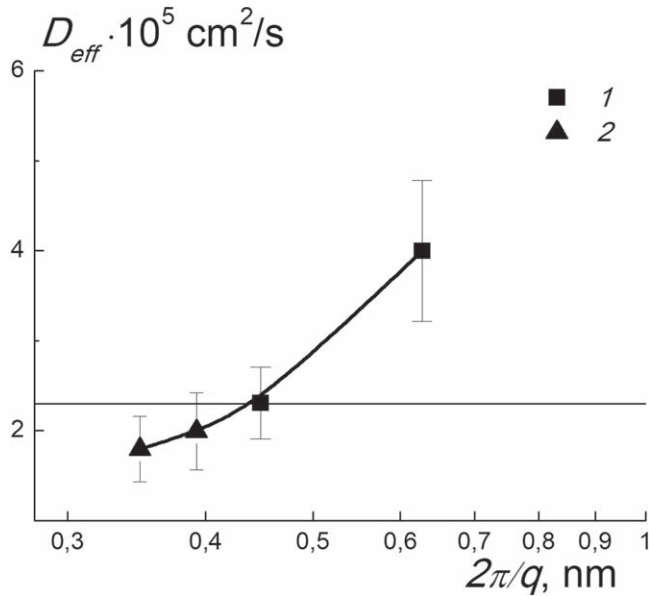
Figure 6. Effective diffusion constant versus spatial scale in membranes, EW = 800; 1000 (1, 2). Bulk water constant $D_W = 2.3 \times 10^{-5}\,\mathrm{cm^2\,s^{-1}}$ is shown (line).

between SO_3H-groups is less probable than a transport with water molecules to which protons may link via hydrogen bonds. Along with this, a regular structure of conducting channels connected into macroscopic network and stabilized is a crucial condition to provide effective functional properties of membranes. To this purpose we modified the polymer matrices by nanodiamonds with hydrophilic surface. These crystals may serve as the capacitors of protons and assure their migration along the facets.

3.3. Membranes modified by nanodiamonds

Aqueous dispersion of detonation nanodiamonds (DND, concentration ~ 1 wt%, ~ 5 nm in size) has been studied by SANS (Spectrometer 'YuMO', JINR, Dubna, Russia) [12–14]. The aim of experiments was to search systems' ordering due to coulomb interactions of positively charged crystals the surface of which was treated by special technologies [9, 10]. We prepared the sample by five-fold dilution of concentrated system (5%wt) above the critical point of gelation ($c^* \sim 4$ wt%) [9]. Herewith we suspected an assembly of diamonds even below critical concentration c^*. Actually the scattering cross section of dispersion exhibits the behaviors close to Porod's law for the particles with sharp borders and Zimm's law for the chains like linear (Gaussian) polymers, $\sigma(q) \sim q^{-4}$ and $\sigma(q) \sim q^{-2}$ [17] (figure 7). The latter testifies the assembly of DND even in diluted system.

Analyzing the data, we found the distribution $\Phi(R)$ of observed objects over the radii for the model of hard spheres using the ATSAS software [15] (figure 8(a)). The $\Phi(R)$ shows the volume fractions of particles with the radii R.

The intensive peak (maximum at $R_m = 2.1$ nm) corresponds to single particles, but the tail of spectrum $\Phi(R)$ indicates the aggregates ($R \sim 10–20$ nm). Particles' assembly
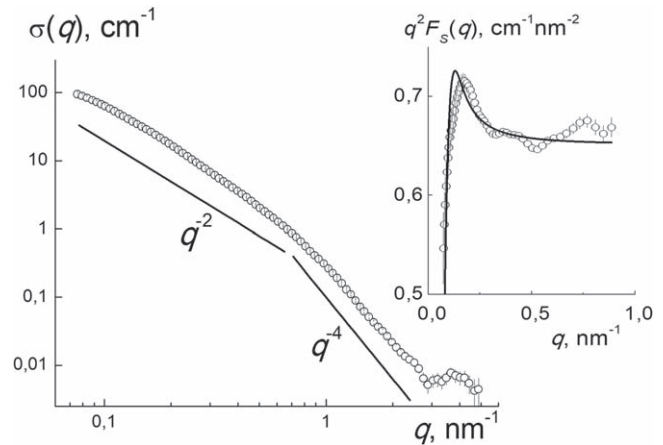

Figure 7. Scattering cross section $\sigma(q)$ of diamonds' aqueous dispersion (1%wt) versus momentum transfer. Lines show characteristic dependencies $\sim q^{-2}$ and q^{-4}. Inset: the structure factor of the dispersion and fitting by the function (4).
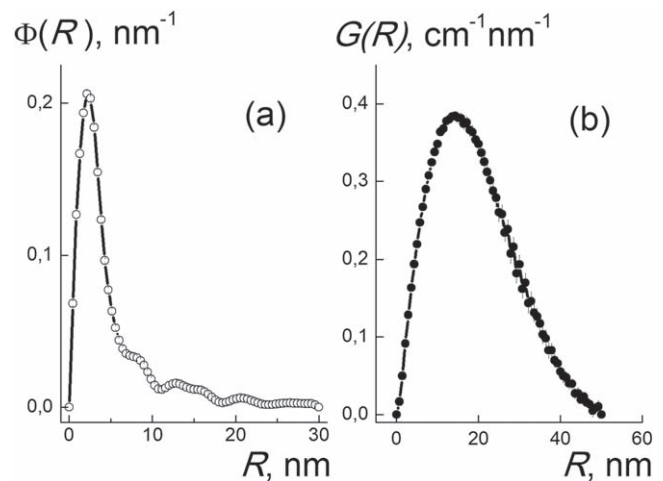
Figure 8. Particles' volume fractions $\Phi(R)$ (a) over the radii R (a), the spectrum of correlations $G(R)$ (b) for DND dispersion.

is described by the structure factor $F_S(q) = \sigma(q)/F^2(q)$ where the squared form-factor of crystals in Guinier approximation $F^2(q) = \exp[-(q r_g)^2/3]$ depends on their gyration radius $r_g = (3/5)^{1/2} R_m = 1.7$ nm (figure 7, inset). In Kratky presentation, the structure factor $q^2 F_S(q)$ shows a major maximum at $q* \sim 0.2$ nm^{-1} indicating spatial correlations between chain aggregates at the distance $\sim 2\pi/q* \sim 30$ nm close to their diameter. This is a result of their contacts in solution when the chains interpenetrate and join into branched structures (figure 7). A junction of chains creates some star-shaped aggregates being basic structural elements in the dispersions of overlapping chains of diamonds. Note, the star-shaped polymers demonstrate scattering pattern in Kratky presentation with a maximum. Its amplitude increases proportionally to the number of arms in star (functionality). The position of maximum is defined by reciprocal gyration radius of stars [22]. To apply this model for the description of the structure of
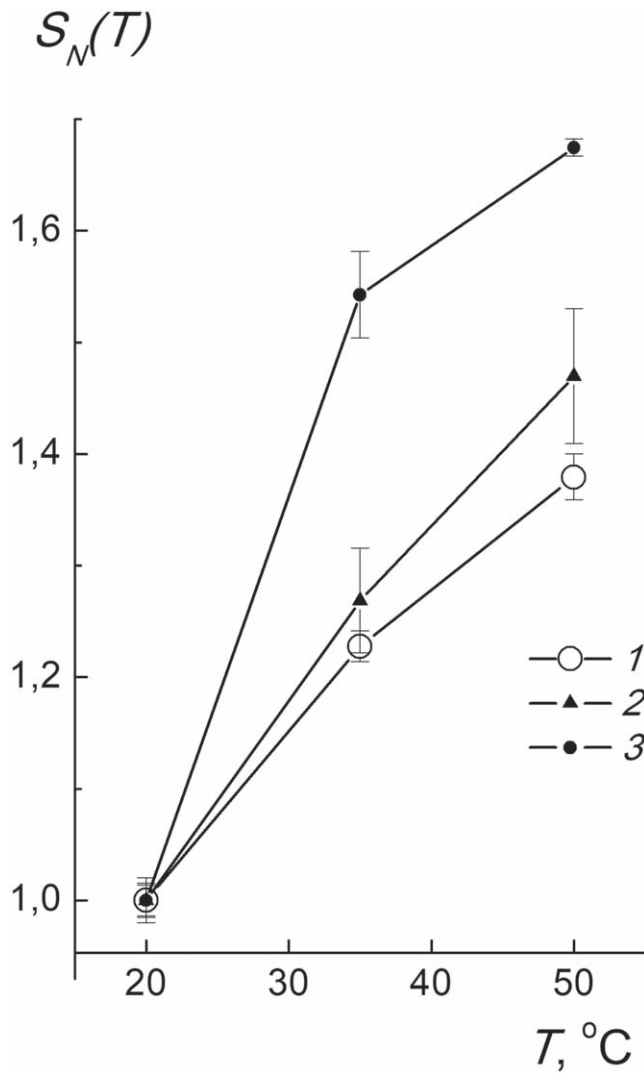
Figure 9. Normalized conductivity $S_N(T)$ versus temperature for polymer membrane (1) and composites with 0.25 and 1.0%wt of DND (2,3).

diamond aggregates, we used Benoit scattering function $F_S(q)$ [22] for star-shaped Gaussian polymers (4)

$$F_S = \frac{2S_o}{z^2}(F_1 + F_2 + F_3), \tag{4}$$

$$F_1 = \frac{f(f-1)}{2}\exp\left(-\frac{2z}{f}\right), \, F_2 = -f(f-2)\exp\left(-\frac{z}{f}\right)$$

$$F_3 = z + \frac{f(f-3)}{2}.$$

where the variable $z = (qR_{GA})^2 f$ depends on the gyration radius R_{GA} of the arm in star with the functionality f that is the number of arms joint at the center, the parameter $S_o = K_d^2$ $\varphi(fv_d n_d)$ depends on the contrast factor for diamond in water (K_d), their volume fraction in dispersion (φ), the volume of a diamond crystal (v_d) and the number of diamonds in each chain (n_d) integrated in star-shaped structure (number of arms f). So the parameter S_o is proportional to the dry volume of star-shaped structure, $V_{dry} = fv_d n_d$. The data were fitted by the function (4) with a variation of the parameters S_o, f, R_{GA} (figure 7, inset).
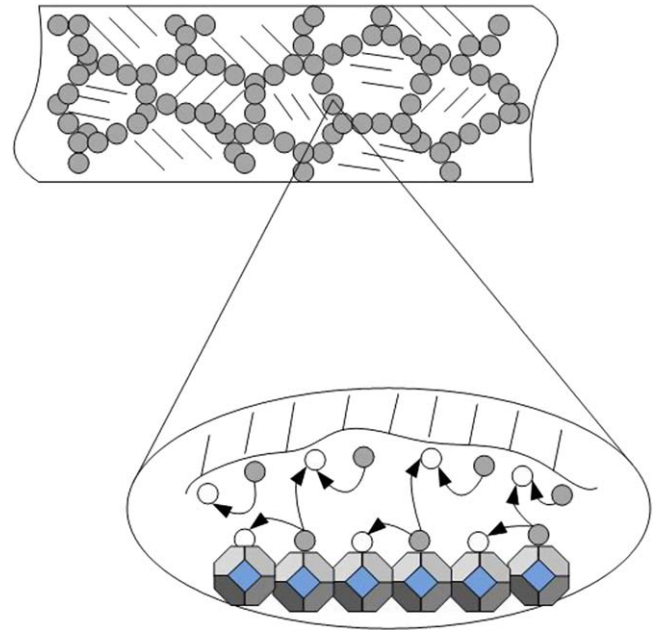
Figure 10. Interface 'polymer-diamond' in composite membranes reinforced by DND crystals providing additional proton conductivity along facets.

This model approximates the data roughly (shift between simulated and experimental peaks) (figure 7, inset). It does not take into account a possible spread in the parameters of aggregates. Nevertheless, this result testifies a formation of star-shaped structures having in average the functionality of centers $f = 3.32 \pm 0.02$ and the arms with the gyration radius $R_{GA} = 8.0 \pm 0.2$ nm. Their end-to-end distance, $h_A = \sqrt{6}R_{GA} = 19.5 \pm 0.4$ nm, defines stars' diameter $d_{ST} \sim 2h_A \sim 40$ nm.

These findings are confirmed in the analysis using the spectrum $G(R) = R^2\gamma(R)$ where the $\gamma(R)$ is the function of correlations between two particles at the distance R (figure 8(b)). The peak of $G(R)$ has the position of maximum $R_{mg} \sim 15$ nm showing a length of correlations in the system. Actually this length is close to the the radius of star-shaped structure, $R_{mg} \sim h_A$, and peak's full width $\sim 2R_m \sim 40$ nm corresponds to its diameter $\sim 2h_A$.

Well organized diamonds ensembles may serve to modify polymer membranes and improve their conductivity, strength and stability at high temperatures. To produce the composites, we used the analog of Aquivion (EW = 890) and the DND with COOH groups grafted to diamond surface. Both components were dissolved dimethylformamide. Further we obtained the composite films by casting the mixed solutions on a glass substrate and removing the solvent. Finally, we prepared the membranes with diamonds' concentrations of 0.25; 1.0%wt and the reference sample without additive.

Even at very low amount (0.25%wt), the DND has induced a gain in conductivity by 3%–10%comparatively to pure polymer. A remarkable temperature effect we observed in the range 20 °C–50 °C where the composites (0.25; 1.0%wt) showed the growth of normalized conductivity $S_N(T) = S(T)/S(20\,°C)$ by $\sim50\%$and $\sim70\%$ respectively while the pure matrix demonstrated a gain of $\sim40\%$ (figure 9).

This promising result for desirable applications of membranes at higher temperatures ($T > 130\,^{\circ}C$) should be treated in connection with structural changes in polymer matrix altered due to the appearance of the interfaces 'polymer-diamond' (figure 10).

DND's embedding into polymer matrix has created highly developed hydrophilic interface polymer-diamond. Wherein the facets of crystals carry COOH ionic groups which may promote in conductivity. In sum, it intensifies a proton migration because of large total area of crystal surfaces serving as conducting walls of slit-shaped channels for diffusion. Along with this, this can stimulate proton hopping from one SO_3H group to another in polymer chains exchanging with protons localized on the sites of crystals (figure 10).

4. Conclusions

In neutron scattering experiments there were found the regularities in structuring membrane polymers having proton conducting channels detected by contrast variation using samples' swelling in light and heavy water. In wet membranes the NSE-method allowed observe fast (picosecond) dynamics involving water diffusion and possible proton hopping at the scales comparable to water molecular size. For better proton conductivity the membrane polymers have been doped with nanodiamonds strongly assembled in solutions into branched structures to be fixed in polymer matrix. In the prepared composites at a low crystalline fraction ($\sim$1%wt) we achieved the substantial gain in conductivity at the enhanced temperatures ($50\,^{\circ}C$) due to the developed conducting interface between diamonds and polymer. The obtained results demonstrate really effective way to regulate nanoscale structure of membranes to design new materials with higher functional properties.

Acknowledgements

References

[1] Kulvelis Y V, Lebedev V T, Trunov V A, Primachenko O N, Khaikin S Y, Torok G and Ivanchev S S 2012 *Pet. Chem.* **52** 565
[2] Primachenko O N *et al* 2018 *Rus. J. Appl. Chem.* **91** 110
[3] Mauritz K A and Moore R B 2004 *Chem. Rev.* **104** 4535
[4] Stassi A *et al* 2011 *J. Power Sources* **196** 8925
[5] Antonucci P L, Ariso A S, Creti P, Rammuni E and Antinucci V 1999 *Solid State Ion.* **125** 431
[6] Baradie B, Dodelet J P and Guay P J 2000 *Electroanal. Chem.* **498** 101
[7] Postnov V N *et al* 2017 *Russ. J. Gen. Chem.* **87** 2754
[8] Hou H *et al* 2013 *Intern. J. Hydrog. Energy* **38** 3346
[9] Vul A Y, Eidelman E D, Aleksenskiy A E, Shvidchenko A V, Dideikin A T, Yuferev V S, Lebedev V T, Kul'velis Y V and Avdeev M V 2017 *Carbon* **114** 242
[10] Lebedev V T, Kulvelis Y V, Kuklin A I and Vul A Y 2016 *Condens. Matter.* **1** 1
[11] Agmon N 1995 *Chem. Phys. Lett.* **244** 456
[12] Kuklin A I *et al* 2011 *J. Phys.:Conf. Ser.* **291** 012013
[13] Kuklin A I, Islamov A K and Gordeliy V I 2005 *Neutron News* **16** 16
[14] Soloviev A G, Solovjeva T M, Ivankov O I, Soloviov D V, Rogachev A V and Kuklin A I 2017 *J. Phys.:Conf. Ser.* **848** 012020
[15] Svergun D I 1992 *J. Crystallogr.* **25** 495
[16] Svergun D I and Feigin L A 1987 *Structure Analysis by Small-Angle x-Ray and Neutron Scattering* ed G W Taylor (New York and London: Plenum Press) ch 2
[17] de Gennes P G 1979 *Scaling Concepts in Polymer Physics* (Itaca and London: Cornel University Press) ch 1
[18] Maccarthy D W, Mark J E and Schaefer D W 1998 *J. Polym. Sci.* B **36** 1167
[19] Mezei F (ed) 1980 Neutron Spin Echo *Proceedings of a Laue-Langevin Institute Workshop* 128 (vol 128) *(Grenoble, October 15-16, 1979)* Lecture Notes in Physics Springer
[20] Mezei F, Pappas C and Gutberlet T (ed) 2003 *Neutron Spin Echo Spectroscopy. Basics, Trends and Applications* (Berlin: Springer)
[21] Bee M 1988 *Quasielastic Neutron Scattering (Bristol, Philadelphia)* ed A Hilger p 373
[22] Rawiso M 1999 *J. Phys.* IV **9** Pr1–147